

PAPER • OPEN ACCESS

Dependence of the polycarbonate mechanical performances on boron nitride flakes morphology

To cite this article: Emanuele Lago *et al* 2021 *J. Phys. Mater.* **4** 045002

View the [article online](#) for updates and enhancements.




The Electrochemical Society
Advancing solid state & electrochemical science & technology
2021 Virtual Education

Intensive Short Courses

Sunday, October 10 & Monday, October 11

Providing students and professionals with in-depth education on a wide range of topics

[CLICK HERE TO REGISTER](#)





PAPER

OPEN ACCESS

RECEIVED
31 March 2021

REVISED
25 May 2021

ACCEPTED FOR PUBLICATION
11 June 2021

PUBLISHED
12 July 2021

Original content from
this work may be used
under the terms of the
[Creative Commons
Attribution 4.0 licence](#).

Any further distribution
of this work must
maintain attribution to
the author(s) and the title
of the work, journal
citation and DOI.



Dependence of the polycarbonate mechanical performances on boron nitride flakes morphology

Emanuele Lago^{1,2} , Peter S Toth^{1,3}, Silvia Gentiluomo^{1,2}, Sanjay B Thorat^{1,4}, Vittorio Pellegrini^{1,4}
and Francesco Bonaccorso^{1,4,*}

¹ Graphene Labs, Istituto Italiano di Tecnologia, via Morego 30, 16163 Genoa, Italy

² Dipartimento di Chimica e Chimica Industriale, Università degli Studi di Genova, via Dodecaneso 31, 16146 Genoa, Italy

³ Department of Physical Chemistry and Materials Science, University of Szeged, Rerrich sq. 1., Szeged 6720, Hungary

⁴ BeDimensional SpA, Lungotorrente Secca, Genoa 30R 16163, Italy

* Author to whom any correspondence should be addressed.

E-mail: francesco.bonaccorso@bedimensional.it

Keywords: hexagonal-boron nitride, liquid phase exfoliation, polymer composite, aspect ratio

Abstract

A key requirement for the exploitation of two-dimensional (2D)-crystals in the field of composites relies on their large-scale production. In this respect, liquid phase exfoliation of layered-crystals is emerging as one of the most promising approaches for the scalable production of high-quality 2D-crystals. However, the dependence of the 2D crystal flakes morphology, i.e. thickness and lateral size, on the mechanical properties of the polymer composites is not fully understood yet. Herein, we tackle this issue by designing an environmentally friendly approach, based on the exfoliation of bulk hexagonal-boron nitride (*h*-BN), widely used as filler in polymer composites for its high intrinsic stiffness, i.e. approaching 1 TPa, in a water/surfactant solution with controlled thickness and lateral size by using cascade ultra-centrifugation. Our approach allows us to obtain two populations of flakes with aspect ratio, i.e. lateral size over thickness, equal to 250 and 350, respectively. The *h*-BN flakes with tuned aspect ratio are subsequently used as filler in a polycarbonate (PC) matrix by exploiting solution blending in 1,3-dioxolane, a solvent with Hansen's solubility parameters matching the ones of *h*-BN, thus enhancing the dispersion of the filler inside the matrix, as evaluated by Raman mapping. We tested the composite mechanical properties finding that flakes with higher aspect ratio show superior reinforcements in terms of both ultimate tensile strength and Young's modulus, compared with their lower aspect ratio counterparts. As example, at 0.1 wt% of loading, the difference in reinforcement in terms of Young's Modulus is of 56 MPa, being the increment, compared to pristine PC, of ~22% for composites produced with higher aspect ratio fillers, whereas it is instead of only ~17% for lower aspect ratio fillers.

1. Introduction

Liquid phase exfoliation (LPE) of layered-materials [1, 2] paved the way towards the large scale exploitation of two-dimensional (2D)-crystals in polymer composite applications [3, 4]. The working principle of LPE relies on the breaking of the inter-sheet forces between layers of a bulk-layered material [3, 5, 6]. The mechanical energy is provided by either shear [7] or ultrasounds [1] in the presence of a stabilizing solvent, peeling off individual layers from the bulk crystal counterpart, resulting in dispersions of defect-free and un-functionalized nanosheets [8]. This top-down method is in principle applicable to all layered materials and it has been already used for obtaining several 2D-crystals such as graphene [7], hexagonal-boron nitride (*h*-BN) [1, 8], molybdenum disulfide (MoS₂) [1, 8], tungsten disulfide (WS₂) [1, 8], indium selenide [9], and black phosphorous [10–12], just to cite a few. The effectiveness of the LPE process, that can be defined by the ratio between the weight of exfoliated and dispersed flakes and the one of the starting bulk-layered material [3, 5, 8], depends mostly on the chosen solvent [3, 5, 8]. In fact, solvents with a surface tension

matching the surface energy of the flakes [3, 5, 8], having Hansen's solubility parameters—HSPs—(i.e. the energy from dispersion forces between molecules (δ_D), the energy from hydrogen bonds between molecules (δ_H), and the energy from dipolar intermolecular force between molecules (δ_P)) [13] similar to the one of the flakes are able to both exfoliate the bulk-layered materials and disperse/stabilize against re-aggregation the exfoliated flakes [1, 3, 14].

In the last years, *h*-BN has attracted increasing attention due to its significant properties, complementary to the ones of graphene [3, 8]. A single layer of *h*-BN has a honeycomb lattice composed by alternating boron (B) and nitrogen (N) atoms, held together by polar covalent bonds [15, 16]. This structure makes single layer *h*-BN mechanically strong, i.e. its Young's modulus (*E*) approaches 1 TPa [17], with a tensile strength of 150 GPa [17] and in-plane stiffness of 267 N m⁻¹ [15]. Contrary to graphene, *h*-BN has no optical absorption in the visible region [15] and it is an electrical insulator having a band-gap of ~6 eV [15]. This set of properties makes *h*-BN appealing for its use as filler in polymer composites [18–22]. Polymer reinforcement has already been achieved with *h*-BN flakes, exfoliated by LPE, in cases of several matrices, such as polyvinyl alcohol (PVA) [23], polymethyl methacrylate [24], polyethylene terephthalate [25], polyvinyl chloride (PVC) [26], and polycarbonate (PC) [27], in which increments of *E* are in the range of 20%–30% compared to the neat matrixes at filler loadings of 0.1 wt% (0.3 wt % for [18]). Usually, for loading of *h*-BN flakes higher than 0.1 wt% the mechanical performances of composites saturate or even decrease, probably due to agglomeration of the flakes dispersed in the polymeric matrixes [23, 25, 28, 29]. On the one hand, occurrence of aggregates, indeed, has been reported in the 0.1–0.2 vol% (~0.2–0.4 wt%) loading range for PVA [23] and PVC [26] based composites, both produced by solvent blending. On the other hand, for composites produced by melt blending, as in the case of [24], agglomeration of fillers can be observed even at lower concentrations, i.e. 0.017 vol% (~0.03 wt%).

It is worth noting that in order to produce 2D-crystal based composites with the targeted mechanical reinforcement, both the dispersion of the fillers in the polymer matrix [30, 31] and their aspect ratio [28, 32–34], i.e. lateral size over thickness, are of paramount importance, as shown both by mathematical models [35, 36] and experimental evidences obtained in the case of graphene flakes [28, 35–39]. A study on the reinforcement of a polymer matrix related to the aspect ratio and dispersion of *h*-BN flakes is, however, still lacking. Therefore, in this work, we tackled this issue by designing *h*-BN flakes with different aspect ratio (250 and 350) exploiting LPE in a water/surfactant solution as the dispersing agent. The exfoliated *h*-BN flakes have been sorted by aspect ratio exploiting sedimentation-based separation (SBS) [3, 29, 40, 41] using a cascade centrifugation [42], obtaining two population of flakes with different morphology, i.e. thickness and lateral size. The as-produced flakes are then integrated into PC-based composites, with varying concentration from 0 to 5 wt%, by means of solution blending, a technique which allows a better dispersion of the flakes in the polymer matrix compared to melt blending [43, 44], by dispersing both PC and *h*-BN flakes in the same solvent, i.e. 1,3-dioxolane. The dispersions are then coagulated in water forming composite pellets, which are finally hot-pressed to produce composite thin films (thickness ~100 μm). Mechanical tests on the composite films have shown significant reinforcements compared to the bare PC polymer, with an increment of ~22% in *E* at 0.1 wt% of loading of *h*-BN flakes with the highest aspect ratio (i.e. 350), while at the same loading the observed increment is of ~17% for the *h*-BN flakes of lower aspect ratio (i.e. 250). A maximum reinforcement of 27% in *E* is further obtained by using high-aspect ratio flakes (i.e. 350) at 0.5 wt% of loading, while the same increment has been reported by a two-fold loading increase for graphene flakes [29].

2. Results and discussion

2.1. Environmentally friendly LPE of *h*-BN and flakes morphology tuning

Large volume production of 2D-crystals, as required for their exploitation in the composite field [3], can be achieved by means of LPE of their bulk counterparts [1, 3]. For many 2D-crystals, such as graphene, WS₂, MoS₂, and *h*-BN, just to cite a few, suitable solvents for their exfoliation, such as dimethylformamide [1, 3, 8], N-methyl-2-pyrrolidone [1, 3, 8], and ortho-dichlorobenzene [1, 3, 8, 45], have surface tension in the 35–40 mN m⁻¹ range [1, 3]. Unfortunately, the majority of these solvents have high boiling points, i.e. more than 150 °C [5], experiencing also toxicological issues [3]. Pure water, due to its surface tension value (72 mN m⁻¹) [46], is generally not appropriate for the dispersion of 2D-crystals [3]. In fact, although a few attempts for its use in an LPE process have been undertaken [47, 48], the achieved concentrations are very low compared to the aforementioned organic solvents. In fact, ~0.1 mg ml⁻¹ has been reported for the case of *h*-BN with 25 h sonication time [47] and ~0.0065 mg ml⁻¹ and ~0.018 mg ml⁻¹ in the case of graphene and *h*-BN, respectively, by using temperature control during the ultra-sonication process [48]. As for example, it has been shown that the stability of exfoliated single- (SLG) and few-layer graphene flakes (FLG) in pure water depends on the balance of repulsive (electrostatic, due to ion absorption) and attractive (van der Waals and hydrophobic interactions) forces [49]. Attractive forces intensify with the increase of the layers

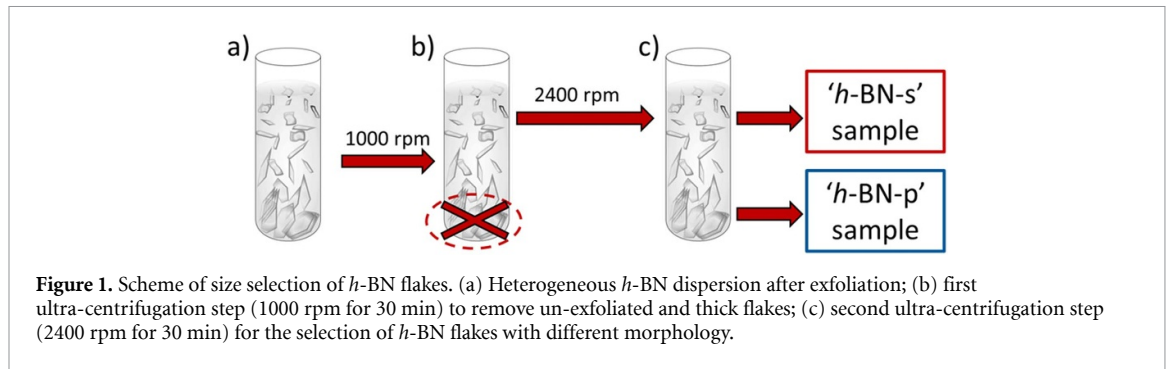


Figure 1. Scheme of size selection of *h*-BN flakes. (a) Heterogeneous *h*-BN dispersion after exfoliation; (b) first ultra-centrifugation step (1000 rpm for 30 min) to remove un-exfoliated and thick flakes; (c) second ultra-centrifugation step (2400 rpm for 30 min) for the selection of *h*-BN flakes with different morphology.

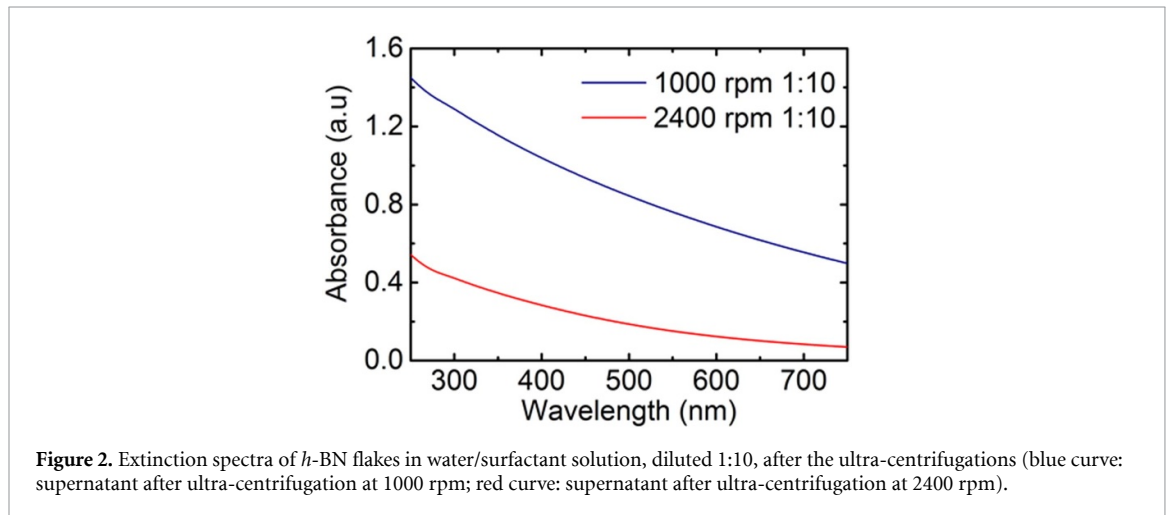


Figure 2. Extinction spectra of *h*-BN flakes in water/surfactant solution, diluted 1:10, after the ultra-centrifugations (blue curve: supernatant after ultra-centrifugation at 1000 rpm; red curve: supernatant after ultra-centrifugation at 2400 rpm).

number, thus FLG flakes are less stable in water compared to SLG ones [49]. Exfoliation yield, defined as the ratio between the weight of dispersed flakes and that of the starting bulk material [5], in water can be increased using additives, such as surfactants [50], which stabilizes exfoliated flakes against re-aggregation [50–53]. Therefore, herein we carried out exfoliation of bulk *h*-BN powder in a water/surfactant solution, selecting Kolliphor® P188 as a surfactant. Kolliphor® P188, also referred as Pluronic® F68 or Lutrol® F68 according to different suppliers, is a triblock copolymer of the family of poloxamers [54, 55] composed by a hydrophobic poly(propylene oxide) central chain, that is attracted to the *h*-BN basal plane through hydrophobic interactions [53], surrounded by two hydrophilic poly(ethylene oxide) chains, which stabilize the exfoliated flakes by steric hindrance [53]. After the exfoliation process a heterogeneous dispersion of *h*-BN flakes is obtained (figure 1(a)). Consequently, a first ultra-centrifugation at 1000 rpm, corresponding to 200 g, (figure 1(b)) has been performed in order to remove all the un-exfoliated and thick *h*-BN flakes [5, 40, 41, 56]. The supernatant is collected by pipetting and subjected to a second ultra-centrifugation step (figure 1(c)) at 2400 rpm, corresponding to 1000 g. Both supernatant and precipitate (re-dispersed in a fresh water/surfactant solution) are collected and named as '*h*-BN-s' and '*h*-BN-p', in which 's' and 'p' correspond to 'supernatant' and 'precipitate', respectively.

The concentration of 2D-crystal dispersions are usually measured exploiting optical extinction spectroscopy (OES) [1, 3]. The measured extinction (A) is correlated to the concentration of the 2D-crystal flakes by the Lambert-Beer law: $A = \alpha lc$, in which l (m) is the light path length, c (mg ml^{-1}) is the concentration of dispersed flakes, and α ($\text{ml mg}^{-1} \text{m}^{-1}$) is the extinction coefficient. The latter for *h*-BN has been calculated by Coleman *et al* to be $2367 \text{ ml mg}^{-1} \text{m}^{-1}$ at 300 nm wavelength [1]. Extinction spectra of the collected supernatants after the ultra-centrifugations are shown in figure 2. The calculated concentration of *h*-BN flakes is therefore 0.62 mg ml^{-1} after the first ultra-centrifugation step (blue curve in figure 2) and 0.19 mg ml^{-1} after the second one (red curve in figure 2).

In order to exploit the solution blending technique for the fabrication of the composite, both polymer matrix and inorganic fillers have to be dispersed in the same solvent and mixed together [29, 43]. Therefore, *h*-BN-s and *h*-BN-p flakes have been re-dispersed in 1,3-dioxolane, the solvent used for dissolving the PC matrix, and their aspect ratio is evaluated measuring lateral size and thickness of the flakes using transmission electron microscopy (TEM, figure 3) and atomic force microscopy (AFM, figure 4). Figures 3(a) and (c) show the representative transmission electron micrographs of *h*-BN-s and *h*-BN-p flakes, respectively, whereas the

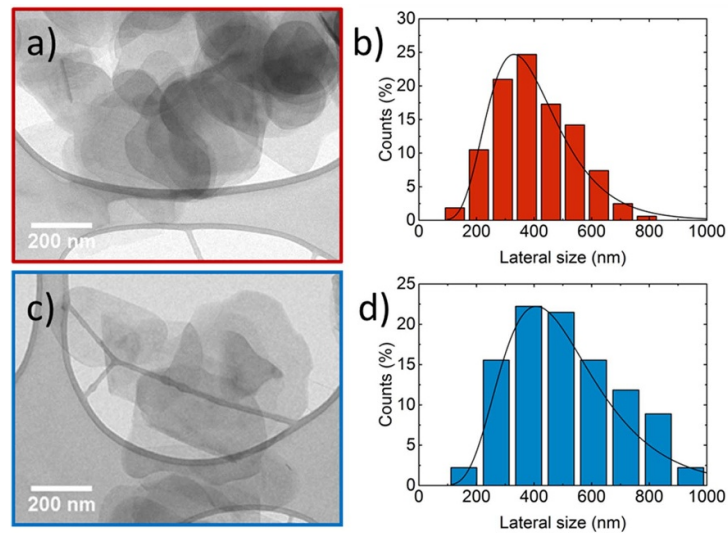


Figure 3. Transmission electron microscopy analysis on *h*-BN flakes. (a) Representative TEM micrograph of *h*-BN-s flakes re-dispersed in 1,3-dioxolane; (b) statistical analysis from TEM micrographs of the *h*-BN-s flakes lateral size; (c) representative TEM micrograph of *h*-BN-p flakes re-dispersed in 1,3-dioxolane and (d) statistical analysis from TEM micrographs of the *h*-BN-p flakes lateral size.

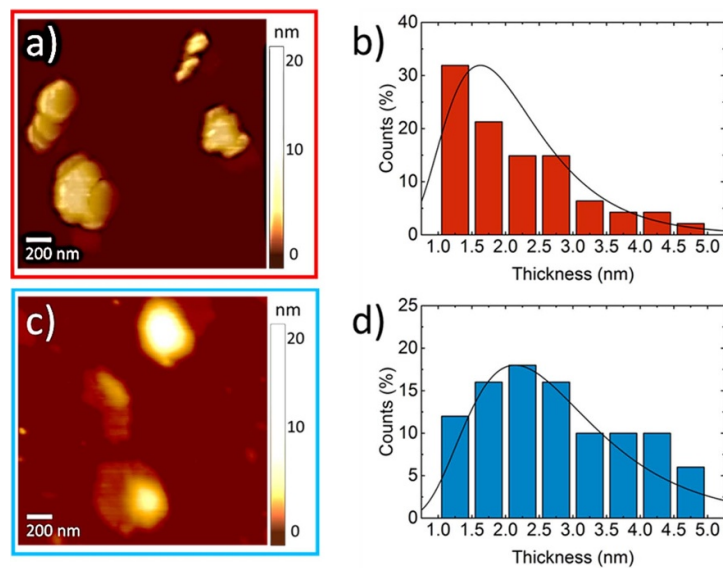


Figure 4. Atomic force microscopy analysis on *h*-BN flakes. (a) Representative AFM image of BN-s flakes re-dispersed in 1,3-dioxolane; (b) statistical analysis from AFM images of the *h*-BN-s flakes thickness; (c) representative AFM image of *h*-BN-p flakes re-dispersed in 1,3-dioxolane and (d) statistical analysis from AFM images of the *h*-BN-p flakes thickness.

corresponding statistical analyses (based on 100 flakes) on lateral size are shown in figures 3(b) and (d). The statistics are fitted by a log-normal distribution [57] with most probable values of lateral size, assessed as the maximum measured length of the flake, peaked at 340 nm for *h*-BN-s flakes and 410 nm for *h*-BN-p flakes.

In figures 4(a) and (c), the representative AFM images are shown for the *h*-BN-s and *h*-BN-p samples, respectively, and relative statistical analysis on thickness are shown in figures 4(b) and (d). The statistics are fitted by a log-normal distribution with most probable values of thickness peaked at 1.6 nm for *h*-BN-s flakes and 2.3 nm for *h*-BN-p flakes. Liquid phase exfoliated *h*-BN single layer has an apparent height of ~ 1 nm on Si/SiO₂ wafer [1, 47], whereas theoretical spacing between *h*-BN layers is 0.33 nm [15, 47]. Based on the aforementioned considerations, we can estimate the average number of the layer for each sample from their AFM thickness being ~ 3 for *h*-BN-s and ~ 5 for the *h*-BN-p sample. Using the lateral size values obtained by TEM analysis, the calculated aspect ratios are, consequently, ~ 350 for *h*-BN-s and ~ 250 for *h*-BN-p.

Raman spectroscopy is a useful tool for characterizing 2D-crystals [3, 8, 58], In plane atomic displacements give origin to two Raman active E_{2g} modes in *h*-BN [16], a low frequency mode at

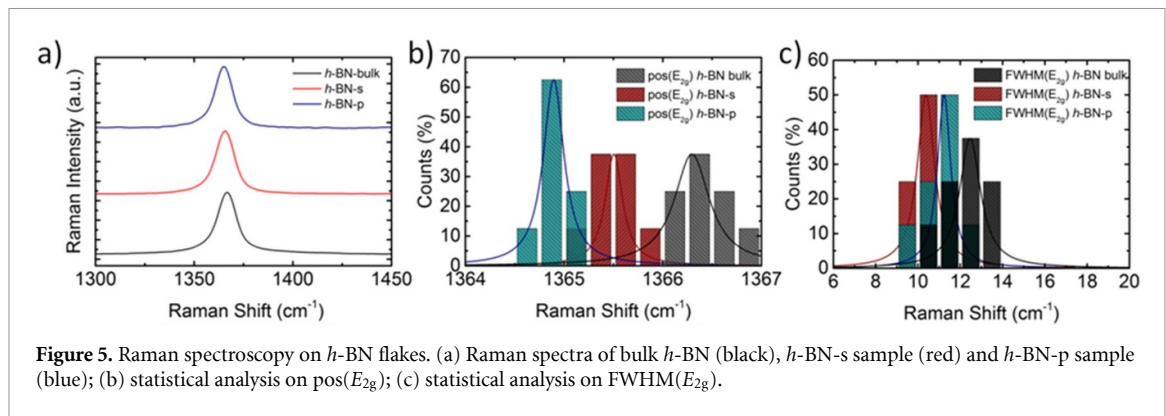


Figure 5. Raman spectroscopy on *h*-BN flakes. (a) Raman spectra of bulk *h*-BN (black), *h*-BN-s sample (red) and *h*-BN-p sample (blue); (b) statistical analysis on pos(E_{2g}); (c) statistical analysis on FWHM(E_{2g}).

Table 1. Summary of HSPs and surface tension at 25 °C for PC [13], 1,3-dioxolane [13, 68], chloroform [13, 69], THF [13, 70], and *h*-BN [1]. For *h*-BN is reported as surface tension the one of a solvent that matches its surface energy.

Materials	δ_D (MPa ^{1/2})	δ_P (MPa ^{1/2})	δ_H (MPa ^{1/2})	Surface tension (mN m ⁻¹)
PC	19.1	10.9	5.1	—
1,3-dioxolane	18.1	6.6	9.3	32.6 [68]
Chloroform	17.8	3.1	5.6	27.1 [69]
THF	16.8	5.7	8.0	26.4 [70]
<i>h</i> -BN	17–19	4–10	4–10	35

49–52.5 cm⁻¹ [16, 59], assigned to shear-type rigid layer mode of the crystal [16, 59], and a high frequency mode at 1366 cm⁻¹ [16, 60]. For example, for *h*-BN monolayer produced by micromechanical cleavage (MC), a blue shift up to 4 cm⁻¹ has been observed, due to the hardening of E_{2g} phonons [16, 60], with possible red shifts due to strain by the MC preparation method, which eventually further red shifts for the bilayer *h*-BN (by ~1–2 cm⁻¹) [16, 60]. In figure 5 is presented the Raman analysis carried out on the *h*-BN dispersions. Figure 5(a) shows representative spectra acquired on bulk *h*-BN (black trace), *h*-BN-s sample (red trace) and *h*-BN-p sample (blue trace) in which the E_{2g} peaks around 1366 cm⁻¹. The statistical analysis on the shift in the position of high frequency E_{2g} peak (pos(E_{2g})) is reported in figure 5(b). The red shifts of exfoliated samples respect to the bulk *h*-BN reveals the formation of few layer *h*-BN flakes [60, 61]. In particular, the pos(E_{2g}) of *h*-BN-s sample, centred at 1365 cm⁻¹, is attributed to the presence of mostly bilayer and tri-layer flakes for liquid phase exfoliated *h*-BN [61], confirming the results of AFM microscopy. The red shift in few-layer *h*-BN is attributed to the elongation of B–N bonds due to interlayer interactions that involves a softening of the phonons [16, 60, 61]. The full width at half maximum (FWHM) of the E_{2g} peak (figure 5(c)) reduces with the decrease of the flake thickness, starting from 12.5 cm⁻¹ for the *h*-BN bulk powder to 11 cm⁻¹ and 10 cm⁻¹ for the *h*-BN-p and *h*-BN-s samples, respectively. This reduction in E_{2g} peak line-shape is consistent with a decrease in the superposition of multiple peaks due to a more homogeneity of the flakes size compared to the bulk powder, subsequent to the exfoliation and purification process [61].

2.2. Composite preparation and characterization

In order to understand the impact of the *h*-BN flakes morphology on the mechanical properties of PC-based composite, we designed and produced *h*-BN-s/PC and *h*-BN-p/PC composites by solution blending technique in 1,3-dioxolane, as detailed in the experimental section. 1,3-dioxolane is a low boiling point solvent (78 °C) with a set of solubility parameters (i.e., HPS and surface tension) that makes it promising for the dispersion of *h*-BN flakes compared to, for example, tetrahydrofuran (THF) and chloroform (see table 1). In fact, such solvents are able to dissolve PC, being generally used for the production of solution processed 2D-crystals/PC composites [27, 62–64]. 1,3-dioxolane has HSPs that are in the range of the ones proposed by Coleman *et al* for exfoliated *h*-BN [1] and a surface tension that is close to the exfoliated *h*-BN surface energy. Considering these values, by using 1,3-dioxolane as a solvent for the blending, we expected a thorough mixing of the exfoliated *h*-BN flakes inside the PC matrix.

The dispersion of *h*-BN flakes in PC matrix is evaluated by scanning electron microscopy (SEM) in combination with Raman spectroscopy (figure 6). Comparison of scanning electron micrographs of cross section area of composites with the 0.5 wt% of loading (*h*-BN-s/PC in figure 6(a) and *h*-BN-p/PC in figure 6(b)) reveal that fillers—the brighter objects in the images—are uniformly dispersed in the polymeric matrix. Raman spectra on composite films (figure 6(c)) show the presence of peaks belonging to both *h*-BN

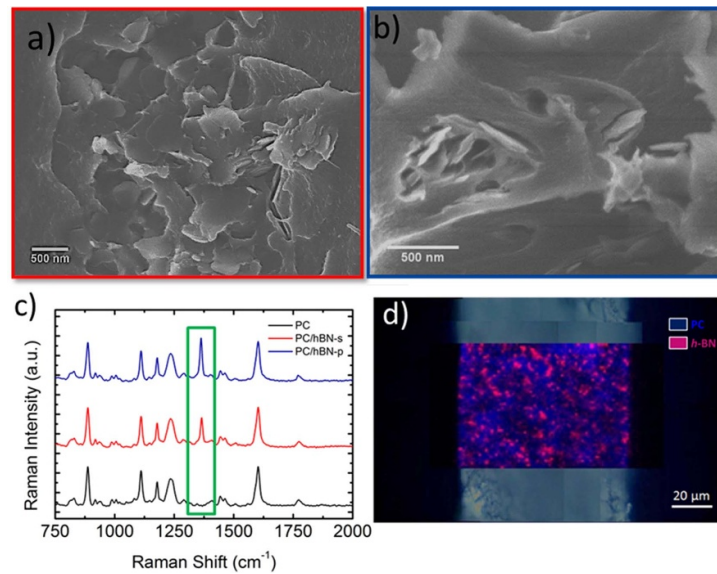


Figure 6. Cross section SEM micrographs of (a) PC/h-BN-s 0.5 wt% and (b) PC/h-BN-p 0.5 wt%. (c) Raman spectra of pristine PC (black trace), PC/h-BN-s 0.5 wt% composite (red trace), PC/h-BN-p 0.5 wt% composite (blue trace); in the green box is displayed the high frequency E_{2g} peak of h-BN ($\sim 1366 \text{ cm}^{-1}$). (d) Raman mapping on a cross section of PC/h-BN-s 0.5 wt% composite showing the acquired Raman signals of PC (blue) and h-BN-s flakes (pink).

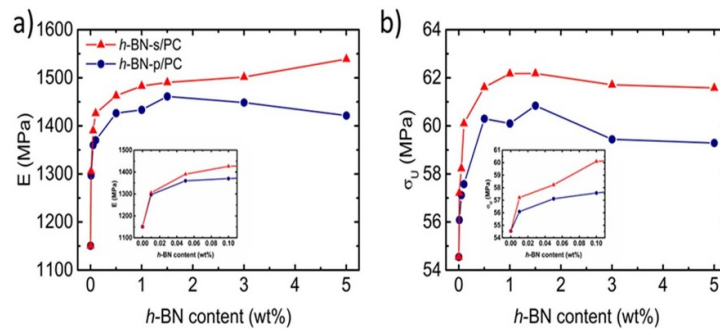


Figure 7. Mechanical performances of composites with h-BN loading. (a) Young's Modulus (E); (b) ultimate tensile strength (σ_U). In the insets of (a) and (b), enlarged part of E and σ_U for 0–0.1 wt% of h-BN contents is presented, respectively.

(displayed in the green box) and PC, revealing the mixing of the h-BN flakes within the polymeric matrix, further confirmed by a Raman mapping made on the film cross-section (figure 6(d)).

The homogeneously dispersed h-BN flakes improved the mechanical properties of the PC matrix. Results obtained from uniaxial tensile testings on composites are presented in figure 7. With the 0.1 wt% of loading (corresponding to 0.06 vol%), E of PC increased from $1165 \pm 56 \text{ MPa}$ of the neat polymer to $1370 \pm 23 \text{ MPa}$ (+17%) and $1426 \pm 76 \text{ MPa}$ (+22%) using as filler h-BN-p and h-BN-s flakes, respectively, see figure 7(a). It is worth noting that a difference in an aspect ratio of 100 reflects a 5% (56 MPa) variation in the reinforcement of the composite. By using the rule of mixtures [65], it is possible to evaluate the effective modulus of the filler (E_F) in the composite. Herein, at this loading, h-BN-s flakes and h-BN-p flakes show an E_F of 436 GPa and 342 GPa, respectively, values that are less than half of the theoretical value of h-BN [17], but, however, in line with the reported literature results [23–26]. A further increase in the aspect ratio of the flakes, still keeping optimized their dispersion in the polymer matrix, can in principle approach E_F to the theoretical value [28]. Moreover, the increment obtained using the h-BN-s flakes is comparable to the one obtained by Sainsbury *et al*, in which methoxyphenyl carbamate-functionalized h-BN flakes have been used as a reinforcing agent for the PC matrix [27]. The functionalization of flakes is able to increase the interfacial stress transfer between filler and polymer chains [27], and a proper entanglement, i.e. their interlocking, can be achieved when the grafted molecules on the flakes are structurally and chemically similar to the matrix [27, 66], thus minimizing their enthalpy of mixing [66]. Nevertheless, flake functionalization requires the addition of one or more experimental steps to the process. It is worth to mention that in the same work, the authors report that no effective reinforcement has been found using untreated h-BN flakes [27]. The

enhancements we obtained using un-functionalized *h*-BN flakes can be attributed to the different solvent used for the solution blending process, i.e. 1,3-dioxolane instead of THF used in [19], which does not match the solubility parameters of *h*-BN, as previously explained (see table 1).

Furthermore, a 27% of increment in *E* has been found at 0.5 wt% of loading of *h*-BN-s flakes, while the same increment is obtained by a two-fold loading increase for graphene [29], reaching finally a + 35% of reinforcing at a loading of 5 wt%. For both samples, however, exceeding the 0.5 wt% of *h*-BN flakes loading, the E_F of the flakes suddenly decreases, e.g. is lower than 100 GPa at 1.0 wt% of loading. This behaviour, often observed in literature for low dimensional fillers [23, 25, 28, 29], is attributed to the occurrence of flakes agglomeration [28, 67].

The ultimate tensile strength (σ_U) of the composite at 0.1 wt% of *h*-BN-s loading is increased of ~12% compared to the neat polymer (60.1 ± 2.1 MPa vs. 54.5 ± 1.9 MPa), whereas composite at 0.1 wt % of *h*-BN-p loading has shown an increment of ~6% (57.6 ± 2.6 MPa), see figure 7(b). Exceeding the loading of 0.5 wt%, for both fillers, there is no more evidence of strength reinforcement in composites and even we report a slight decrease for loadings higher than 1.5 wt%. This fact is consistent with the evoked agglomeration issues found at the same loadings for *E*.

The *h*-BN-s flakes, with higher aspect ratio compared to the *h*-BN-p flakes, gave also the highest reinforcements, both in terms of *E* and σ_U for all the investigated concentrations (0.01–5 wt% range). The differences are highlighted in the insets to figures 7(a) and (b) that focus the *h*-BN flake loadings up to 0.1 wt%.

3. Conclusion

We have demonstrated the dependence of the *h*-BN flakes morphology, i.e. thickness and lateral size, on the mechanical properties of PC/*h*-BN composites. Bulk *h*-BN powder has been exfoliated using LPE in a water/surfactant solution. *h*-BN flakes have been sorted by aspect ratio (i.e. lateral size vs. thickness) using a cascade centrifugation and exploiting the SBS process, obtaining two different specimens *h*-BN-s and *h*-BN-p with aspect ratios of 350 and 250 and an average number of layers of 3 and 5, respectively, as measured by AFM. These flakes have been used as filler for the production of composites with enhanced mechanical properties using PC as a matrix. Composites have been produced by means of solution blending, dissolving PC in 1,3-dioxolane, a solvent with a surface tension and HSPs that match the ones required for *h*-BN exfoliation and stabilization. This allows a thorough dispersion of flakes inside the polymer matrix, as confirmed by Raman spectroscopy and SEM. The differences in aspect ratio of the fillers reflected in differences in the obtained mechanical reinforcements. The composites produced by using the fillers with higher aspect ratio have shown the highest mechanical performances, both in terms of stiffness (evaluated measuring *E*, e.g. +22% compared to the pristine PC matrix obtained at 0.1 wt% of loading of *h*-BN-s flakes vs. +17% obtained at the same loading of *h*-BN-p flakes) and strength (evaluated measuring σ_U , e.g. +12% respect the pristine PC matrix obtained at 0.1 wt% of loading of *h*-BN-s flakes vs. +6% obtained at the same loading of *h*-BN-p flakes). Moreover, the combination of high aspect ratio fillers and the use of 1,3-dioxolane as a solvent for the blending with the polymeric matrix, allow us to obtain for PC-based composites increments in mechanical properties comparable with the ones of functionalized *h*-BN flakes [27] and even higher if compared with composites having liquid phase exfoliated-graphene flakes as filler [29]. The high-yield water/surfactant exfoliation herein proposed, together with the size selection of *h*-BN flakes and their subsequent use as reinforcing agent in a polymer matrix, can boost the exploitation of 2D crystals for large-scale commercial applications.

4. Methods

4.1. Materials

PC pellets (MAKROLON®2405), *h*-BN powder (Sigma Aldrich, ~1 μ m particle size, 98%), Kolliphor® P 188, acetone (ACS Reagent, $\geq 99.5\%$) and 1,3-dioxolane (Reagent Plus®, 99%) are purchased from Sigma-Aldrich and used as received.

4.2. Production of the *h*-BN dispersion in 1,3-dioxolane

About 500 mg of *h*-BN powder are dispersed in 50 ml of water/Kolliphor® P188 solution concentrated at 2 wt% and exfoliated in an ultrasonic bath (VWR) for 6 h at full power. Then, the dispersion is ultracentrifuged at 1000 rpm (200 g) for 30 min at a temperature of 15 °C with an ultra-centrifuge (Beckman Coulter Optima™ XE-90, which is equipped with an SW32 Ti rotor), to remove thicker and/or un-exfoliated flakes. The supernatant is collected and ultra-centrifuged again at 2400 rpm (1000 g) for 30 min at 15 °C. A process of solvent exchange is carried out for the re-dispersions of the exfoliated flakes in

1,3-dioxolane, using a rotary evaporator (Heidolph Hei-Vap). After the evaporation of water/surfactant solution, powders are collected and washed for three times with acetone to remove the surfactant residual. This process is carried out using a compact centrifuge (Sigma). The washing step is repeated and the flakes are finally dispersed in 50 ml of 1,3-dioxolane, fine-tuning its concentration at 10 mg ml^{-1} .

4.3. *h*-BN flakes characterization

The morphological characterization (lateral size and thickness) of *h*-BN dispersions is performed by TEM (Jeol JEM 1011) and AFM (Bruker Innova®) on the samples once drop-casted onto holey carbon coated copper grids and Si/SiO₂ wafers, respectively. Statistical analyses on thickness and lateral size are performed measuring ~ 100 flakes from both AFM and TEM images, respectively, and they are fitted with log-normal distributions [57]. The concentration of flakes is investigated by OES using a spectrophotometer (Agilent Cary Varian 5000 UV–Vis). Raman spectra of *h*-BN dispersions, drop casted on Si/SiO₂ wafers, are carried out using a confocal Raman microscope (Renishaw inVia), with an excitation line of 532 nm (2.33 eV), a $50\times$ objective and a controlled incident power of 1 mW on the sample. For the statistical analysis, 15 spectra are collected and peaks are fitted with the Lorentzian function.

4.4. Composite preparation

The *h*-BN/PC composites are produced by using solution blending technique, exploiting a reported procedure [29]. Briefly, PC pellets are dissolved in 1,3-dioxolane, at a concentration of 150 mg ml^{-1} , by stirring for 3 h using a magnetic stirrer. Specified amounts of dispersion are mixed with either *h*-BN-s or *h*-BN-p flakes dispersed in 1,3-dioxolane, obtaining composite dispersions for both samples ranging from 0 to 5 wt% of filler compared to the polymer. After mixing, composite dispersions are subsequently sonicated for 1 h obtaining a thorough mixing and then coagulated/precipitated forming pellets by pouring into water. Composite pellets are then dried in a vacuum oven (Binder VDL 115) for 12 h at 80 °C and finally hot pressed at 2 tons at 225 °C for 5 min using a press (Madatec Atlas T8) in order to produce composite films of $\sim 100 \mu\text{m}$ thickness.

4.5. Composite characterization

The morphology of the composite is investigated by using scanning electron microscopy (FE-SEM Joel GSM-7500FA). Raman spectra of the composite materials are acquired using a confocal Raman microscope and using the experimental conditions detailed in section 4.3. The mechanical properties of composite films are measured using a universal testing machine (Instron dual column tabletop 3365), with 5 mm min^{-1} cross-head speed. The tensile measurements are carried out, according to ASTM D882 Standard Test Methods for tensile properties of thin plastic film, on five different specimens for each film.

Data availability statement

All data that support the findings of this study are included within the article (and any supplementary files).

Acknowledgments

The authors thank Simone Lauciello for performing HR-SEM measurements. This project has received funding from the European Union's Horizon 2020 research and innovation program under Grant Agreement No. 881603-GrapheneCore3, from the European Union's MSCA-ITN ULTIMATE project under Grant Agreement No. 813036 and the Bilateral project GINSENG between NSFC (China) and MAECI (Italy) (2018–2020), by Natural Science Foundation of Shandong Province (Grant No. ZR2019QEM009).

ORCID iDs

Emanuele Lago  <https://orcid.org/0000-0002-1812-6993>

Francesco Bonaccorso  <https://orcid.org/0000-0001-7238-9420>

References

- [1] Coleman J N *et al* 2011 Two-dimensional nanosheets produced by liquid exfoliation of layered materials *Science* **331** 568–71
- [2] Del Rio Castillo A E *et al* 2018 High-yield production of 2D crystals by wet-jet milling *Mater. Horizons* **5** 890–904
- [3] Ferrari A C *et al* 2014 Science and technology roadmap for graphene, related two-dimensional crystals, and hybrid systems *Nanoscale* **7** 4598–810
- [4] Valorosi F *et al* 2020 Graphene and related materials in hierarchical fiber composites: production techniques and key industrial benefits *Compos. Sci. Technol.* **185** 107848

- [5] Bonaccorso F, Lombardo A, Hasan T, Sun Z, Colombo L and Ferrari A C 2012 Production and processing of graphene and 2d crystals *Mater. Today* **15** 564–89
- [6] Li Z et al 2020 Mechanisms of liquid-phase exfoliation for the production of graphene *ACS Nano* **14** 10976–85
- [7] Paton K R et al 2014 Scalable production of large quantities of defect-free few-layer graphene by shear exfoliation in liquids *Nat. Mater.* **13** 624–30
- [8] Bonaccorso F, Bartolotta A, Coleman J N and Backes C 2016 2D-crystal-based functional inks *Adv. Mater.* **28** 6136–66
- [9] Petroni E et al 2018 Liquid-phase exfoliated indium-selenide flakes and their application in hydrogen evolution reaction *Small* **14** 1800749
- [10] Hanlon D et al 2015 Liquid exfoliation of solvent-stabilized few-layer black phosphorus for applications beyond electronics *Nat. Commun.* **6** 8563
- [11] Del Río Castillo A E, Pellegrini V, Sun H, Buha J, Dinh D A, Lago E, Ansaldo A, Capasso A, Manna L and Bonaccorso F 2018 Exfoliation of few-layer black phosphorus in low-boiling-point solvents and its application in Li-ion batteries *Chem. Mater.* **30** 506–16
- [12] Del Río Castillo A E, Reyes-Vazquez C D, Rojas-Martinez I E, Thorat S B, Serri M, Martinez-Hernandez A L, Velasco-Santos C, Pellegrini V and Bonaccorso F 2019 Single-step exfoliation and functionalization of few-layers black phosphorus and its application for polymer composites *FlatChem* **18** 100131
- [13] Hansen C 2007 *Hansen Solubility Parameters: A User's Handbook* (Boca Raton, FL: CRC Press)
- [14] Del Río-Castillo A E, Merino C, Díez-Barra E and Vázquez E 2014 Selective suspension of single layer graphene mechanochemically exfoliated from carbon nanofibres *Nano Res.* **7** 963–72
- [15] Lin Y and Connell J W 2012 Advances in 2D boron nitride nanostructures: nanosheets, nanoribbons, nanomeshes, and hybrids with graphene *Nanoscale* **4** 6908–39
- [16] Pakdel A, Bando Y and Golberg D 2014 Nano boron nitride flatland *Chem. Soc. Rev.* **43** 934–59
- [17] Mortazavi B and Cuniberti G 2014 Mechanical properties of polycrystalline boron-nitride nanosheets *RSC Adv.* **4** 19137–43
- [18] Meng W et al 2014 Polymer composites of boron nitride nanotubes and nanosheets *J. Mater. Chem. C* **2** 10049–61
- [19] Joy J, George E, Haritha P, Thomas S and Anas S 2020 An overview of boron nitride based polymer nanocomposites *J. Polym. Sci.* **58** 3115–41
- [20] Chaurasia A, Verma A, Parashar A and Mulik R S 2019 Experimental and computational studies to analyze the effect of h-BN nanosheets on mechanical behavior of h-BN/polyethylene nanocomposites *J. Phys. Chem. C* **123** 20059–70
- [21] Li S, Yang T, Zou H, Liang M and Chen Y 2017 Enhancement in thermal conductivity and mechanical properties via large-scale fabrication of boron nitride nanosheets *High Perform. Polym.* **29** 315–27
- [22] Farooq M U, Jan R, Azeem M, Umer M A, Akram M A, Khan A N, Ahmad I, Khan S A, Umar Z A and Liaqat U 2020 Enhanced mechanical properties of functionalized BN nanosheets-polymer composites *J. Polym. Res.* **27** 1–9
- [23] Khan U, May P, O'Neill A, Bell A P, Boussac E, Martin A, Semple J and Coleman J N 2013 Polymer reinforcement using liquid-exfoliated boron nitride nanosheets *Nanoscale* **5** 581–7
- [24] Zhi C, Bando Y, Tang C, Kuwahara H and Golberg D 2009 Large-scale fabrication of boron nitride nanosheets and their utilization in polymeric composites with improved thermal and mechanical properties *Adv. Mater.* **21** 2889–93
- [25] Xie S, Istrate O M, May P, Barwich S, Bell A P, Khan U and Coleman J N 2015 Boron nitride nanosheets as barrier enhancing fillers in melt processed composites *Nanoscale* **7** 4443–50
- [26] Jan R, May P, Bell A P, Habib A, Khan U and Coleman J N 2014 Enhancing the mechanical properties of BN nanosheet-polymer composites by uniaxial drawing *Nanoscale* **6** 4889–95
- [27] Sainsbury T, Satti A, May P, O'Neill A, Nicolosi V, Gun'ko Y K and Coleman J N 2012 Covalently functionalized hexagonal boron nitride nanosheets by nitrene addition *Chem.—A Eur. J.* **18** 10808–12
- [28] May P, Khan U, O'Neill A and Coleman J N 2012 Approaching the theoretical limit for reinforcing polymers with graphene *J. Mater. Chem.* **22** 1278–82
- [29] Lago E, Toth P S, Pugliese G, Pellegrini V and Bonaccorso F 2016 Solution blending preparation of polycarbonate/graphene composite: boosting the mechanical and electrical properties *RSC Adv.* **6** 97931–40
- [30] Kuilla T, Bhadra S, Yao D, Kim N H, Bose S and Lee J H 2010 Recent advances in graphene based polymer composites *Prog. Polym. Sci.* **35** 1350–75
- [31] Huang X, Qi X, Boey F and Zhang H 2012 Graphene-based composites *Chem. Soc. Rev.* **41** 666–86
- [32] Palermo V, Kinloch I A, Ligi S and Pugno N M 2016 Nanoscale mechanics of graphene and graphene oxide in composites: a scientific and technological perspective *Adv. Mater.* **28** 6232–8
- [33] Cataldi P et al 2016 Effect of graphene nano-platelet morphology on the elastic modulus of soft and hard biopolymers *Carbon* **109** 331–9
- [34] Zahid M, Del Río Castillo A E, Thorat S B, Panda J K, Bonaccorso F and Athanassiou A 2020 Graphene morphology effect on the gas barrier, mechanical and thermal properties of thermoplastic polyurethane *Compos. Sci. Technol.* **200** 108461
- [35] Halpin Affdl J C and Kardos J L 1976 The Halpin-Tsai equations: a review *Polym. Eng. Sci.* **16** 344–52
- [36] Fornes T D and Paul D R 2003 Modeling properties of nylon 6/clay nanocomposites using composite theories *Polymer* **44** 4993–5013
- [37] Zhao X, Zhang Q, Chen D and Lu P 2010 Enhanced mechanical properties of graphene-based poly(vinyl alcohol) composites *Macromolecules* **43** 2357–63
- [38] Rafiee M A, Rafiee J, Wang Z, Song H, Yu Z-Z and Koratkar N 2009 Enhanced mechanical properties of nanocomposites at low graphene content *ACS Nano* **3** 3884–90
- [39] Gong L, Kinloch I A, Young R J, Riaz I, Jalil R and Novoselov K S 2010 Interfacial stress transfer in a graphene monolayer nanocomposite *Adv. Mater.* **22** 2694–7
- [40] Maragó O M et al 2010 Brownian motion of graphene *ACS Nano* **4** 7515–23
- [41] Hassoun J et al 2014 An advanced lithium-ion battery based on a graphene anode and a lithium iron phosphate cathode *Nano Lett.* **14** 4901–6
- [42] Backes C et al 2016 Production of highly monolayer enriched dispersions of liquid-exfoliated nanosheets by liquid cascade centrifugation *ACS Nano* **10** 1589–601
- [43] Kim H, Kobayashi S, AbdurRahim M A, Zhang M J, Khusainova A, Hillmyer M A, Abdala A A and Macosko C W 2011 Graphene/polyethylene nanocomposites: effect of polyethylene functionalization and blending methods *Polymer* **52** 1837–46
- [44] Kim H, Miura Y and Macosko C W 2010 Graphene/polyurethane nanocomposites for improved gas barrier and electrical conductivity *Chem. Mater.* **22** 3441–50

- [45] Toth P S *et al* 2016 Asymmetric MoS₂ /graphene/metal sandwiches: preparation, characterization, and application *Adv. Mater.* **28** 8256–64
- [46] Israelachvili J N 2011 *Intermolecular and Surface Forces* 3rd edn (New York: Academic)
- [47] Lin Y, Williams T V, Xu T-B, Cao W, Elsayed-Ali H E and Connell J W 2011 Aqueous dispersions of few-layered and monolayered hexagonal boron nitride nanosheets from sonication-assisted hydrolysis: critical role of water *J. Phys. Chem. C* **115** 2679–85
- [48] Kim J *et al* 2015 Direct exfoliation and dispersion of two-dimensional materials in pure water via temperature control *Nat. Commun.* **6** 8294
- [49] Bepete G, Anglaret E, Ortolani L, Morandi V, Huang K, Pénicaud A and Drummond C 2016 Surfactant-free single-layer graphene in water *Nat. Chem.* **9** 347–52
- [50] Lotya M *et al* 2009 Liquid phase production of graphene by exfoliation of graphite in surfactant/water solutions *J. Am. Chem. Soc.* **131** 3611–20
- [51] Green A A and Hersam M C 2009 Solution phase production of graphene with controlled thickness via density differentiation *Nano Lett.* **9** 4031–6
- [52] Smith R J *et al* 2011 Large-scale exfoliation of inorganic layered compounds in aqueous surfactant solutions *Adv. Mater.* **23** 3944–8
- [53] Zhu J, Kang J, Kang J, Jariwala D, Wood J D, Seo J-W T, Chen K-S, Marks T J and Hersam M C 2015 Solution-processed dielectrics based on thickness-sorted two-dimensional hexagonal boron nitride nanosheets *Nano Lett.* **15** 7029–36
- [54] Schmolka I R 1973 US 3740421 A
- [55] Bonaccorso F, Hasan T, Tan P H, Sciascia C, Privitera G, Di Marco G, Gucciardi P G and Ferrari A C 2010 Density gradient ultracentrifugation of nanotubes: interplay of bundling and surfactants encapsulation *J. Phys. Chem. C* **114** 17267–85
- [56] Capasso A, Del Rio Castillo A E, Sun H, Ansaldo A, Pellegrini V and Bonaccorso F 2015 Ink-jet printing of graphene for flexible electronics: an environmentally-friendly approach *Solid State Commun.* **224** 53–63
- [57] Kouroupis-Agalou K, Liscio A, Treossi E, Ortolani L, Morandi V, Pugno N M and Palermo V 2014 Fragmentation and exfoliation of 2-dimensional materials: a statistical approach *Nanoscale* **6** 5926
- [58] Ferrari A A C and Basko D D M 2013 Raman spectroscopy as a versatile tool for studying the properties of graphene *Nat. Nanotechnol.* **8** 235–46
- [59] Kuzuba T, Era K, Ishii T and Sato T 1978 A low frequency Raman-active vibration of hexagonal boron nitride *Solid State Commun.* **25** 863–5
- [60] Gorbachev R V *et al* 2011 Hunting for monolayer boron nitride: optical and Raman signatures *Small* **7** 465–8
- [61] Sainsbury T, Satti A, May P, Wang Z, McGovern I, Gun'ko Y K and Coleman J N 2012 Oxygen radical functionalization of boron nitride nanosheets *J. Am. Chem. Soc.* **134** 18758–71
- [62] Li D, Del Rio Castillo A E, Jussila H, Ye G, Ren Z, Bai J, Chen X, Lipsanen H, Sun Z and Bonaccorso F 2016 Black phosphorus polycarbonate polymer composite for pulsed fibre lasers *Appl. Mater. Today* **4** 17–23
- [63] Yoonessi M and Gaier J R 2010 Highly conductive multifunctional graphene polycarbonate nanocomposites *ACS Nano* **4** 7211–20
- [64] Sain P K, Goyal R K, Prasad Y V S S, Sharma K B and Bhargava A K 2015 Few-layer-graphene/polycarbonate nanocomposites as dielectric and conducting material *J. Appl. Polym. Sci.* **132** 42443
- [65] Rosenthal J 1992 A model for determining fiber reinforcement efficiencies and fiber orientation in polymer composites *Polym. Compos.* **13** 462–6
- [66] Rubinstein M and Colby R H 2003 *Polymer Physics* (Oxford: Oxford University Press)
- [67] Coleman J N, Khan U, Blau W J and Gun'ko Y K 2006 Small but strong: a review of the mechanical properties of carbon nanotube-polymer composites *Carbon* **44** 1624–52
- [68] Calvo E, Pintos M, Amigo A and Bravo R 2004 Surface tension and density of mixtures of 1,3-dioxolane+alkanols at 298.15 K: analysis under the extended Langmuir model *J. Colloid Interface Sci.* **272** 438–43
- [69] Weiss G 1986 *Hazardous Chemicals Data Book* (Park Ridge, NJ: Noyes Data Corp)
- [70] Flick E W 1985 *Industrial Solvents Handbook* (Park Ridge, NJ: Noyes Publications)